Title

Templated Synthesis of End-Functionalized Graphene Nanoribbons through Living Ring-Opening Alkyne Metathesis Polymerization

Journal

Journal of the American Chemical Society, 141(28)

ISSN

0002-7863

Authors

von Kugelgen, Stephen
Piskun, Ilya
Griffin, James H
et al.

Publication Date

2019-07-17

DOI

10.1021/jacs.9b01805

Peer reviewed

Templated Synthesis of End-Functionalized Graphene Nanoribbons Through Living Ring-Opening Alkyne Metathesis Polymerization

Stephen von Kugelgen,[†] Ilya Piskun,[†] James H. Griffin,[†] Christopher T. Eckdahl,[†] Nanette N. Jarenwattananon[†] and Felix R. Fischer[†,∫,|,*]

[†]Department of Chemistry, University of California Berkeley, Berkeley, California 94720, United States

[∫]Materials Sciences Division, Lawrence Berkeley National Laboratory, Berkeley, California 94720, United States

[|]Kavli Energy Nanosciences Institute at the University of California Berkeley and Lawrence Berkeley National Laboratory, Berkeley, California 94720, United States

ABSTRACT: Atomically precise bottom-up synthesized graphene nanoribbons (GNRs) are promising candidates for next-generation electronic materials. The incorporation of these highly tunable semiconductors into complex device architectures requires the development of synthetic tools that provide control over the absolute length, the sequence, and the end-groups of GNRs. Here, we report the living chain-growth synthesis of chevron-type GNRs (cGNRs) templated by a *poly*-(arylene ethynylene) precursor prepared through ring-opening alkyne metathesis polymerization (ROAMP). The strained triple bonds of a macrocyclic monomer serve both as the site of polymerization and the reaction center for an annulation reaction that laterally extends the conjugated backbone to give cGNRs with predetermined lengths and end-groups. The structural control provided by a living polymer-templated synthesis of GNRs paves the way for their future integration into hierarchical assemblies, sequence-defined heterojunctions, and well-defined single-GNR transistors via block copolymer templates.

INTRODUCTION

Graphene nanoribbons (GNRs) straddle the border between linear, 1D ladder polymers and extended 2D graphene. While they share a host of the attractive physical and electronic properties of bulk 2D graphene, quantum confinement along one dimension opens a tuneable bandgap that positions GNRs as privileged candidates for next-generation electronic devices. The extremely small (< 2 nm) lateral dimensions, the control of translational symmetry, and the chemical fidelity of edge structures required to manifest these quantum effects in a controlled and reproducible materials system defy traditional top-down synthetic approaches.[1] Bottom-up approaches instead access these narrow strips of graphene from molecular precursors, which allows organic and polymer chemistry to precisely engineer the location of every atom in each repeat unit at the sub-nanometer scale.[2] This strategy has enabled rapid advances in our understanding of the role of nanoribbon width,[3–5] dopant atom incorporation,[6–9] crystallographic symmetry,[10,11] and topological phenomena[12,13] in determining their electronic structure. However, the interface of two or more GNRs of dissimilar electronic band structures fused along a well-defined interface forms the basis of the most promising GNR device architectures.[14,15] While the synthesis of these heterojunctions can be facilitated by hierarchical growth strategies or by scanning probe tip manipulation, the former still yields a statistical distribution of junction interfaces within a single ribbon while the throughput of the latter is extremely limited.[16,17] These tools have proven adequate when small populations of single-junction GNRs are needed to study their electronic interfaces by single molecule spectroscopy, yet transistor device fabrication demands both high structural fidelity and throughput for realistic device yields. These problems are only magnified when multiple predetermined heterojunctions along a single GNR are desired.

The difficulty of assembling GNR heterojunctions is inherent to the techniques used to assemble polymeric GNR precursors, which to date have exclusively relied on step-growth polymerizations.[18] From a polymer perspective, a GNR heterojunction is analogous to the junction unit of a block copolymer; the logical solution to this statistical challenge is to prepare GNRs using a controlled, ideally living, (co)polymerization.[2] Living ring-opening metathesis polymerization (ROMP) has revolutionized the synthesis of precision polymeric materials and enabled ready access to polymers with control of sequence,[19,20] topology,[21,22] stereoregularity,[23] and self-assembly.[24,25] ROMP has become a valuable tool in polymer synthesis in large part due to its tolerance of complex, polyfunctional side chains. However the unsaturated polymer backbones prepared by ROMP are also primed for post-polymerization elaboration, though this is a far less common strategy.[26–28] In the context of GNR synthesis, olefins are undoubtedly useful polyarylene building blocks, but alkynes are particularly valuable due to their redox equivalence to aromatic sp^2 carbons.[29–33] Ring-opening *alkyne* metathesis polymerization (ROAMP) therefore stands as a privileged technique to prepare alkyne-containing block copolymer precursors amenable to further elaboration of the carbon-carbon triple bonds into controlled GNR heterostructures.

Herein, we describe the development of a ROAMP approach to the living, chain-growth synthesis of polymeric GNR precursors. ROAMP of the macrocylic diyne monomer 1,2,5,6(1,3)-tetrabenzenacyclooctaphane-3,7-diyne (**1**) initiated by a highly selective Mo pincer complex [*p*TolC≡Mo(ONO)O^{t}Bu] (**2**) and terminated by metathesis with a functional ynamine gives end-functionalized *poly*-**1** (Scheme 1). The alkynes of *poly*-**1** can be exhaustively

functionalized by inverse electron demand Diels-Alder reactions and the resulting *poly*-phenylene subsequently cyclodehydrogenated to give fully graphitized **cGNR**s (Figure 2). The ability to prepare GNRs from living precursor polymers opens up the possibility for precision synthesis of higher order GNR structures and lays the foundation for the programmable synthesis of single GNR transistor devices featuring multiple controlled heterojunctions.

RESULTS AND DISCUSSION

A scalable, chromatography-free synthesis of the ring-strained monomer 1,2,5,6(1,3)-tetrabenzenacyclooctaphane-3,7-diyne (**1**)[34] is depicted in Figure 1A. Suzuki cross-coupling of (3-(methoxycarbonyl)phenyl)boronic acid (**3**) with 1-bromo-3-((phenylsulfonyl)methyl)benzene (**4**) yields the intermediate biaryl **5**. Dimerization of **5** under pseudo-high-dilution conditions favour the macrocyclization to bis(α-ketosulfone) **6**. Desulfonylation under mild photoredox catalysis cleanly yields diketone **7**. The same reduction can be performed with zinc powder on larger scales, albeit at the cost of a slight decrease in yield (see Supporting Information). Triflation of the enolate of **7** followed by elimination gives access to the ring-strained macrocylic dialkyne **1** in 33% overall yield from **4**. Single crystals suitable for X-ray analysis were grown from a saturated benzene solution. The two molecules found in the asymmetric unit are depicted in Figure 1B. The average C–C≡C bond angle of the alkynes is 160.1(6)°, marking **1** as the least angle-strained alkyne monomer to be polymerized by ROAMP to date. The nearly planar conformation adopted by the macrocycle reflects a small amount of torsional strain around the biaryl C–C bonds as well (dihedral angle ~16.2(6)°, Figure 1B).

The strained monomer **1** is only sparingly soluble in noncoordinating, aprotic solvents compatible with molybdenum(VI)-based ROAMP catalysts. Concentrated solutions (>5 mM) required for an efficient chain-growth polymerization could only be prepared at elevated temperatures. Exhaustive screening of polymerization conditions revealed that at $T > 60$ °C all previously reported ROAMP catalysts were unable to discriminate between the strained alkynes in **1** and the unstrained alkynes in the growing polymer backbone leading to stochastic chain-transfer and -termination processes.[22,35–39] Efforts to increase the kinetic selectivity by lowering the reaction temperature or monomer concentration slowed the rate of polymerization to a crawl; at [**1**] of 2 mM, a 10% loading of the reported ROAMP catalyst [*p*-TolC≡Mo(ONO)(OR)]•KOR (R = $CCH_3(CF_3)_2$)[38] gave an initial turnover frequency of < 2 d^{-1} at 24 °C. In either case, short oligomers and cyclic polymers dominated the product distribution. In contrast, the more electron-rich molybdenum pincer complex **2** featuring a tert-butoxide supporting ligand shows superb selectivity for the strained alkynes in **1** giving access to linear *poly*-**1** in high yield. SEC analysis reveals that samples of *poly*-**1** prepared with ROAMP catalyst **2** exhibit narrow molecular weight distributions ($Đ$ = 1.2, Figure 2A) and M_n that scale linearly with monomer loading and conversion, consistent with a living chain-growth polymerization mechanism. Matrix-assisted laser desorption ionization time of flight mass spectrometry (MALDI-TOF MS) of *poly*-**1a** (Figure 2B) shows a family of peaks separated by integer repeat units of the monomer mass ($\Delta m/z$ = 352 u). We thus conclude that ROAMP catalyst **2** selectively reacts with strained alkynes in **1** over the unstrained triple bonds in the growing polymer backbone, effectively preventing undesired chain-transfer processes that would lead to cyclic polymers, fractional numbers of monomer units in the growing polymer chain, and a broadening of the molecular weight distribution. Taking advantage of selective chain-transfer reagents derived from ynamine **8**,[40] the living polymer chain ends can be terminated with functional groups to give end-functionalized polymers. NMR end-group analysis and MALDI-TOF MS confirm the incorporation of a single nitrophenyl group per polymer chain (Supporting Information Figure S1).

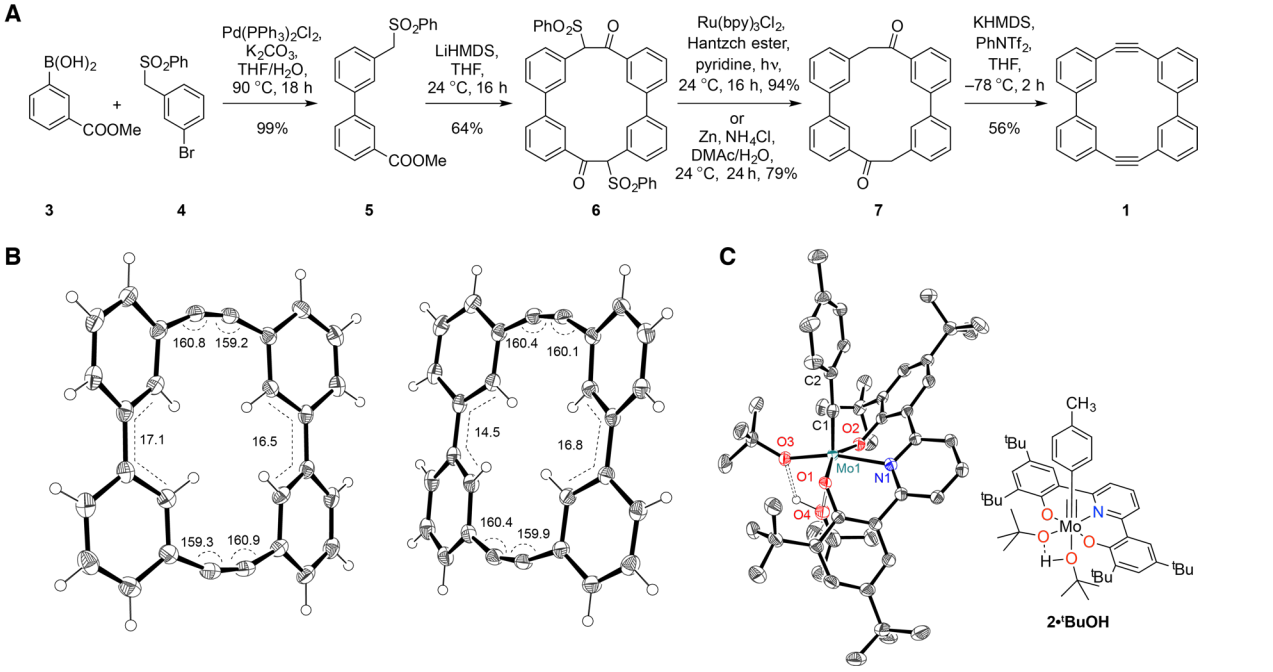

Figure 1. Synthesis and X-ray crystal structure of 1,2,5,6(1,3)-tetrabenzenacyclooctaphane-3,7-diyne (1) and ROAMP catalyst 2. A. Major steps include Suzuki coupling, high-dilution macrocyclization, photoredox desulfonylation, and triflation/elimination to give **1**. B. Single X-ray crystal structure of **1**. C. Single X-ray crystal structure of **2•^{t}BuOH**. Thermal ellipsoids are drawn at the 50% probability level. Colour coding: C (gray), H (white), O (red), N (blue), Mo (turquoise). Hydrogen atoms attached to carbon in **2•^{t}BuOH** and ligand disorder are omitted for clarity.

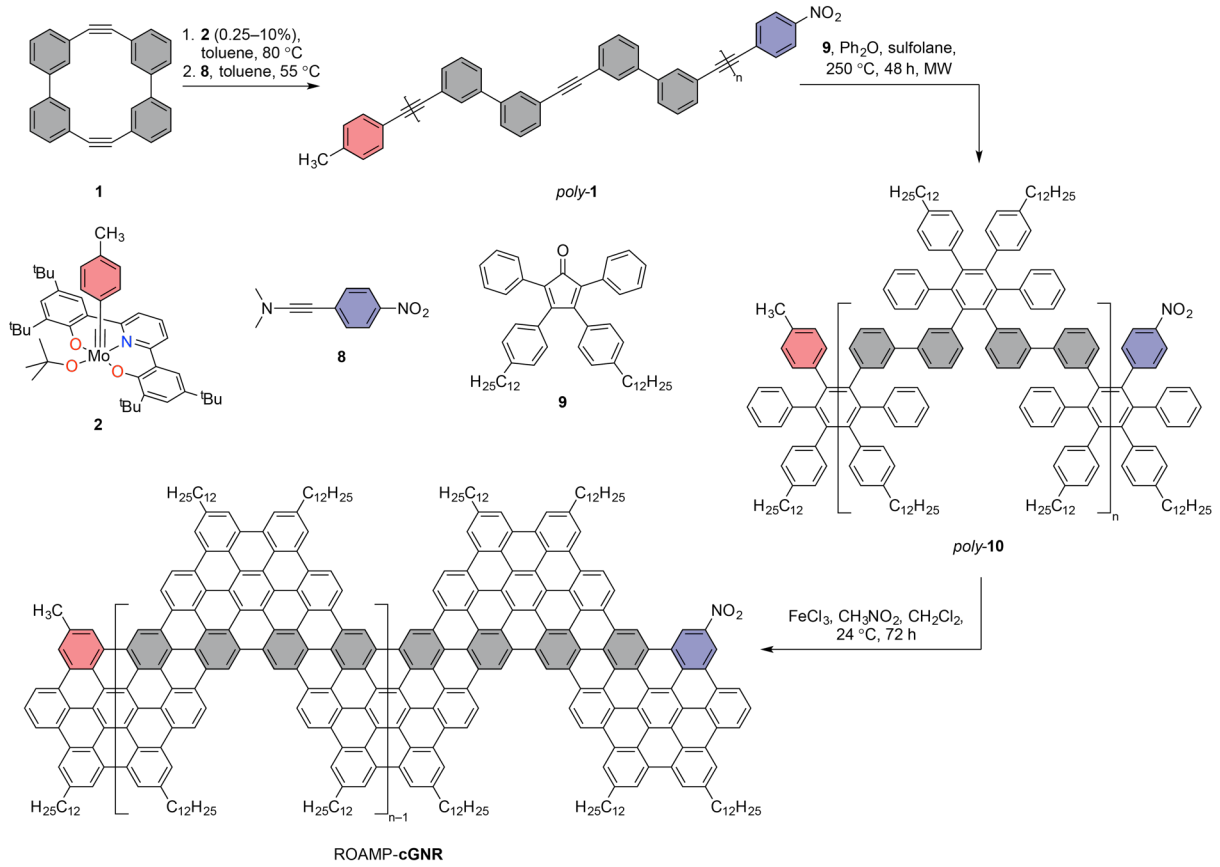

Scheme 1. Ring-opening alkyne metathesis polymerization of 1 and post-polymerization functionalization to give ROAMP-cGNR. ROAMP of **1** with **2** at 80 °C, followed by termination with **8** at 55 °C gives end-functionalized *poly*-**1**. Diels-Alder benzannulation with **9** under microwave irradiation leads to *poly*-**10**. Oxidative cyclodehydrogenation yields the fully graphitized ROAMP-**cGNR**.

With the M_n, $Đ$, and end groups of *poly*-**1** controlled by ROAMP, we turned to the lateral extension of the alkynes to yield the characteristic polyphenylene backbone of a cGNR. We herein relied on the inverse-electron demand Diels-Alder reaction between internal alkynes and 2,3,4,5-tetraarylcyclopentadienones, a robust method commonly used in polyarylene synthesis.[32] Lateral extension of *poly*-**1** with unsubstituted 2,3,4,5-tetraphenylcyclopentadienone leads to incomplete transformations and the precipitation of an insoluble *poly*-phenylene from the reaction mixture. Diels-Alder reaction of *poly*-**1** with cyclopentadienone **9** featuring dodecyl chains at 250 °C in a microwave reactor gave the desired solubilized polyphenylene *poly*-**10**. MALDI-TOF MS of *poly*-**10a** (Figure 2C) shows a new family of ions exhibiting the larger repeat unit mass, with minor ion families due to alkyl chain fragmentation. Size exclusion chromatography (SEC, Figure 2A) reveals an apparent increase in molecular weight along with a slight broadening of the molecular weight distribution. SEC traces of higher molecular weight *poly*-**10b** and *poly*-**10c** derived from *poly*-**1b** (M_n 7 kDa) and *poly*-**1c** (M_n 14 kDa) show a characteristic shoulder. This irreproducible secondary peak could be due to the formation of larger polymer aggregates in the mobile phase ($CHCl_3$).

Critical to any successful post-polymerization strategy is the quantification of the degree of functionalization. This is especially true for the synthesis of cGNRs from *poly*-**1**, as any structural defects induced by incomplete lateral extension will lead to defects in the resulting extended cGNR backbone. Initial solution-state ^{13}C-NMR experiments showed that unfunctionalized alkynes can no longer be detected in a reaction mixture of *poly*-**1** with **9** after as little as 1 h at 250 °C. Even with isotopically labelled substrates, the long T_1 relaxation time of *sp*-hybridized carbon atoms makes the detection of trace alkynes by ^{13}C NMR difficult. To overcome this analytical challenge, we explored chemical methods to detect residual unreacted alkynes in samples of *poly*-**10**. Oxidative cleavage of residual alkynes by e.g. ozonolysis or potassium permanganate proved unsuitable as they slowly degrade the aromatic backbone of *poly*-**10** leading to false-positives even in *poly*-phenylenes prepared by Yamamoto cross-coupling polymerizations. Instead, we turned to highly active alkyne cross-metathesis catalysts such as $[RC{\equiv}Mo(OC(CH_3)(CF_3)_2)_3]$ (R = 4-trifluoromethyphenyl) (**11**) capable of reacting selectively with residual alkynes along the backbone of *poly*-**10** under mild conditions. Alkyne cross-metathesis of samples of *poly*-**10** taken after 1 h, 2 h, and 4 h (SEC traces in Figure 2D) in the presence of a ~100-fold excess of 1,2-bis(4-trifluoromethylphenyl)acetylene show a significant decrease in M_n (Figure 2E) indicative of residual unreacted alkynes in the polymer chain below the detection limit of ^{13}C NMR. A secondary advantage of our depolymerization strategy is that the alkyne metathesis catalyst **11** selectively transfers a 4-trifluoromethylphenyl group to each end of the two resulting polymer fragments that can readily be detected by ^{19}F NMR.

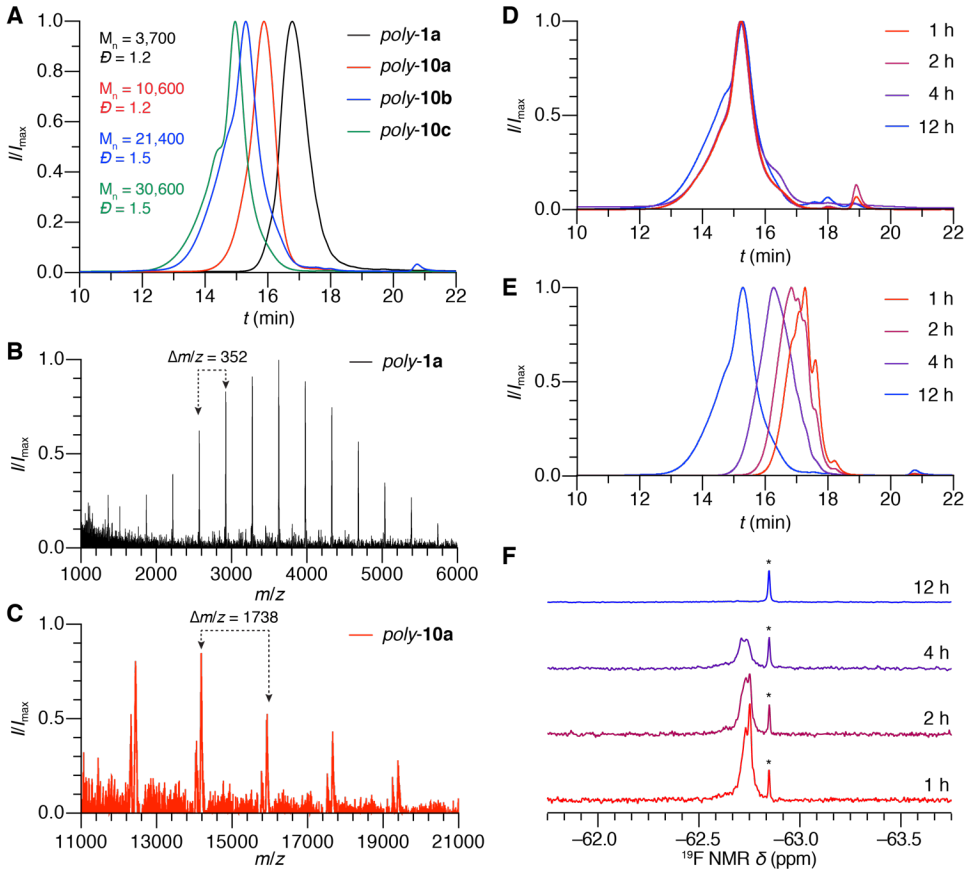

Figure 2. ROAMP of 1 to *poly*-1 and its post-polymerization extension to *poly*-10. A. SEC of *poly*-**1a** and polyphenylenes *poly*-**10a,** *poly*-**10b,** and *poly*-**10c**. **B,C.** MALDI-TOF mass spectrum of *poly*-**1a** and *poly*-**10a** exhibiting the expected repeat unit of 352 u and 1738 u respectively (minor peaks at lower m/z are due to alkyl chain fragmentation). **D.** SEC of *poly*-**10b** taken at 1 h, 2 h, 4 h, and 12 h from the crude Diels-Alder reaction of *poly*-**1** with **9**. **E.** Metathesis depolymerization tests to determine the extent of the Diels-Alder reaction to form *poly*-**10b**. **F.** ^{19}F NMR of *poly*-**10b** samples subjected to depolymerization after Diels-Alder reaction (* denotes residual 1,2-bis(4-trifluoromethylphenyl)acetylene).

Figure 2F shows the ^{19}F NMR traces of depolymerized samples of *poly*-**10** taken at varying reaction times. Integration of the CF_3 ^{19}F NMR signals against an internal standard reveal an average of >25, 19, and 2.5 unreacted alkynes per polymer chain after 1 h, 2 h, and 4 h, respectively. SEC traces of samples of *poly*-**10** taken after 12 h (Figure 2D) no longer show any decrease in the M_n when subjected to alkyne-cross metathesis depolymerization conditions (Figure 2E). ^{19}F NMR spectra of the same samples confirm the absence of signals that could be attributed to the incorporation of 4-trifluoromethylphenyl groups into the polymer chain ends as part of the alkyne-cross metathesis with **11** (Figure 2F). Lastly, we used solid state NMR spectroscopy as an independent method to confirm the exhaustive lateral extension of *poly*-**1** with the cyclopentadienone **9**. The spatial proximity of any residual alkyne carbon atoms to the *ortho* hydrogen atoms of an adjacent aromatic ring (<2.7 Å) should enable their direct observation by cross-polarization solid-state NMR where signal recovery is limited by the much shorter hydrogen T1.[41] The ^{1}H-^{13}C CP-SSNMR spectrum of *poly*-**10a** depicted in Figure 3a lacks the characteristic signatures (80–100 ppm) associated with alkynes. Microwave heating proved critical to the successful and exhaustive lateral extension of *poly*-**1**. If the same reaction was performed in a thermal heating bath, residual alkynes could still be detected even after >21 d. Efforts to drive the thermal reaction to completion at temperatures >260 °C led to the rapid decomposition of cyclopentadienone **9**.

Oxidative cyclodehydrogenation of pristine samples of *poly*-**10** under Scholl reaction conditions yielded ROAMP-**cGNR** as a black powder dispersible in nonpolar organic solvents. Under identical conditions, a small molecule model of the repeat unit of *poly*-**10** gave a single oxidation product consistent with the cGNR backbone (Supporting Information Schemes S1–S2). Solid-state ^{13}C NMR spectroscopy (Figure 3A) further confirms the successful ring-fusion that yields the extended polycyclic aromatic backbone of **cGNR**s. Characteristic resonances of quaternary carbons at 139–141 ppm are shifted to higher field following the lateral fusion of aromatic rings, leaving the downfield resonance for the alkylated GNR carbons visible at 139 ppm. A direct comparison of the Raman spectrum of ROAMP-**cGNR**s (Figure 3B) with an authentic sample of **cGNR**s prepared through Yamamoto step-growth polymerization shows the characteristic signatures of D (1330 cm^{-1}) and G (1610 cm^{-1}) peaks along with the expected 2D (2660 cm^{-1}), D+G (2935 cm^{-1}) overtones. IR spectra of ROAMP-**cGNR**s (Figure 3C) show a dramatic attenuation of the aromatic C–H stretching modes, centered around 3050 cm^{-1} in *poly*-**10**, following the successful oxidative cyclodehydrogenation. UV-Vis spectra of ROAMP-**cGNR**s show a broad visible absorption along with a shoulder centered at ~550 nm characteristic for **cGNR**s.[42] Since these ROAMP-**cGNR**s were prepared from a well-defined, monodisperse precursor polymer (*poly*-**1**), their lengths can be controlled with high precision.

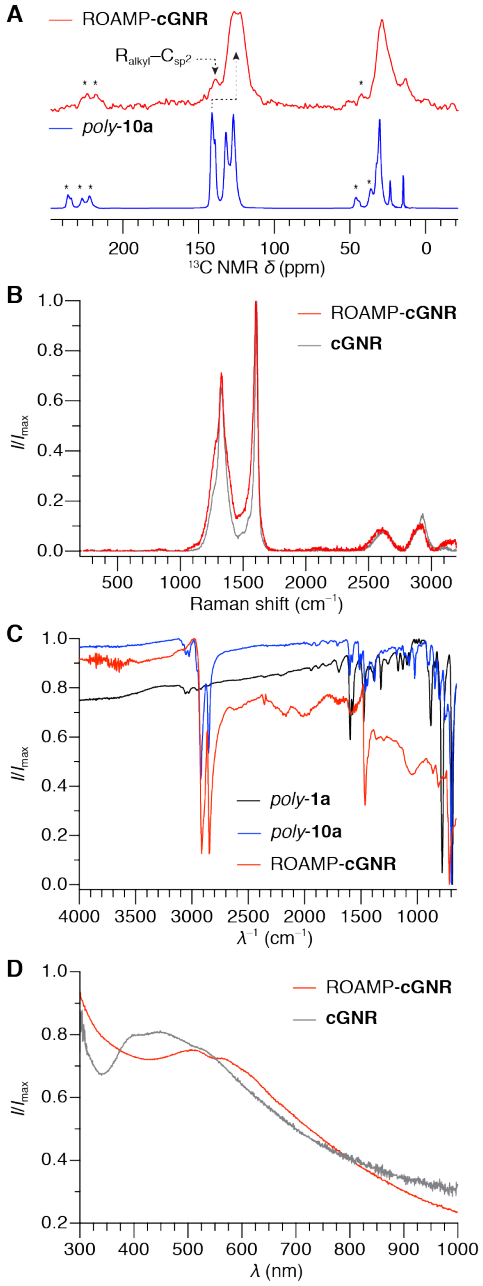

Figure 3. Spectroscopic characterization of *poly*-1, *poly*-10, ROAMP-cGNR, and cGNRs. A. ^{1}H-^{13}C CP-MAS SSNMR spectra of *poly*-**10** and ROAMP-**cGNR**s (*spinning side band) showing the upfield shift of the fused GNR carbon core. **B.** Raman spectra of ROAMP-**cGNR**s and an authentic sample of **cGNR**s prepared through Yamamoto step-growth polymerization (514 nm excitation). **C.** IR (ATR) of *poly*-**1a**, *poly*-**10a**, and ROAMP-**cGNR**s. **D.** UV-Vis spectra of ROAMP-**cGNR**s and **cGNR**s prepared through Yamamoto step-growth polymerization. Dispersions were prepared by sonicating 0.2 mg GNR in 2 mL NMP for 1 h and filtering through glass wool to remove large aggregates.

The chevron GNR backbone derived from *poly*-**1** has a length of 1.7 nm per repeat unit.[43] Oxidation of *poly*-**10c**, derived from ~14 kDa *poly*-**1c** (corresponding to ~40 monomers) thus yields a bulk sample of well-defined **cGNR** featuring atomically defined end groups and a narrow length distribution centered at 68 nm, easily long enough to span lithographically patterned channels in FET device architectures.

CONCLUSION

We have developed a solution-based bulk synthesis of solubilized, end-functional **cGNR**s featuring predictable and narrow molecular weight distributions. The combination of a scalable, chromatography-free synthesis of ring-strained diyne monomer and the exquisite selectivity of a finely tuned Mo benzylidyne ROAMP catalyst gives ready access to precise *poly*-(arylene ethynylene) templates. Lateral Diels-Alder extension of the polymer backbone followed by exhaustive cyclodehydrogenation gives access to the fully graphitized **cGNR**s. The quantitative consumption of all alkynes in the polymer template during Diels-Alder annulation was confirmed independently by solid state NMR and a new metathesis depolymerization technique that proved highly selective for and sensitive to trace residual alkynes. Our living ring-opening alkyne metathesis polymerization approach not only gives access to cGNRs with deterministic control over the ribbon length and end functionality, but the success of these living polymer templates also represents the first step toward the rational synthesis of complex intraribbon GNR heterojunctions from block copolymer templates.

EXPERIMENTAL SECTION

Materials and General Methods. Unless otherwise stated, all manipulations of air and/or moisture sensitive compounds were carried out in oven-dried glassware, under an atmosphere of Ar or N_2. All solvents and reagents were purchased from Alfa Aesar, Spectrum Chemicals, Acros Organics, TCI America, Matrix Scientific, and Sigma-Aldrich and were used as received unless otherwise noted. Organic solvents were dried by passing through a column of alumina and were degassed by vigorous bubbling of N_2 or Ar through the solvent for 20 min. Diphenyl ether was purified by fractional crystallization from the melt. Sulfolane was stirred with powdered KOH (10 %w/v) for 24 h then fractionally distilled under reduced pressure (discarding the first and last 20%). Solid alkyne substrates were recrystallized under N_2 from anhydrous solvents prior to use. For air- and moisture-sensitive NMR, deuterated solvents were stirred 24 h over 10 %w/v drying agent (C_6D_6 and toluene-d_8, CaH_2; $CDCl_3$, P_2O_5) subjected to three freeze-pump-thaw cycles, and vacuum transferred onto activated molecular sieves. Thin layer chromatography was performed using SiliCycle silica gel 60 Å F-254 precoated plates (0.25 mm thick) and visualized by UV absorption. All ^{1}H, ^{13}C{^{1}H}, and ^{19}F NMR spectra were recorded on Bruker AV-600, DRX-500, or AV-500 spectrometers, and are referenced to (residual) solvent peaks ($CDCl_3$ ^{1}H NMR δ = 7.26 ppm, ^{13}C NMR δ = 77.16 ppm; C_6D_6 ^{1}H NMR δ = 7.16 ppm, ^{13}C NMR δ = 128.06 ppm; pyridine-d_5 ^{1}H NMR δ = 7.22 ppm, ^{13}C NMR δ = 150.35 ppm) or hexafluorobenzene (^{19}F NMR δ = –162.90 ppm). Solid-state ^{1}H-^{13}C cross polarization (CP) spectra were collected on a Bruker AV-500 spectrometer equipped with a Bruker 4 mm 1H/X probe, at 11 Tesla and a ^{13}C frequency of 125.7 MHz under 10 and 12 kHz magic-angle spinning (MAS) condition, using a contact time of 3 ms and a pulse delay of 5 s, and proton decoupling by two-pulse phase modulation (TPPM) at an angle of 15° and decoupling field strength of ~60 kHz. The Hartmann-Hahn condition for CP experiments was calibrated on solid adamantane, which was also used as an external ^{13}C chemical shift reference (methine C = 29.46 ppm). High-resolution mass spectrometry (EI) was performed on an Autospec Premier (Waters) sector spectrometer in positive ionization mode. ESI mass spectrometry was performed on a Finnigan LTQFT (Thermo) spectrometer. MALDI mass spectrometry was performed on a Voyager-DE PRO (Applied Biosystems Voyager System 6322) in positive mode using a matrix of dithranol. Elemental analysis (CHN) was performed on a Perkin Elmer 2400 Series II combustion analyzer (values are given in %). Size-exclusion chromatography (SEC) was carried out in 0.75% ethanol-stabilized chloroform on a LC/MS Agilent 1260 Infinity set up with one guard and two Agilent Polypore 300 × 7.5 mm columns at 35 °C. All SEC analyses were performed on 0.2 mg/mL (or 50% of saturated, if soluble <0.2 mg/mL) solutions of polymer in $CHCl_3$. An injection volume of 25 µL and a flow rate of 1 mL min^{-1} were used. Calibration was based on narrow dispersity polystyrene standards ranging from M_w = 100 to

4,068,981 Da. ATR-IR spectra were obtained on a Thermo Nicolet 6700 FTIR. Raman spectra were obtained on a Renishaw inVia Qontor Raman microscope using a 514 nm excitation. X-ray crystallography of **1** was performed on a Rigaku XtaLab equipped with a MicroMax-007HF microfocus rotating anode source (Cu–Kα radiation), a Pilatus 200K detector, and an Oxford Cryostream at 100 K. X-ray crystallography of **2**•^{t}**BuOH** was performed on a Bruker APEX II QUAZAR, using a Microfocus Sealed Source (Incoatec IμS; Mo-Kα radiation), Kappa Geometry with DX (Bruker-AXS build) goniostat, a Bruker APEX II detector, QUAZAR multilayer mirrors as the radiation monochromator, and Oxford Cryostream at 100 K. Crystallographic data were solved with SHELXT, refined with SHELXL-2014, visualized with ORTEP, and finalized with Olex (**1**) or WinGX (**2**). Compounds **3**,[44] **9**,[45] **11**,[39] 1,2-bis(4-trifluoromethylphenyl)acetylene,[46] and authentic samples of unsubstituted **cGNR**s[42] were prepared according to literature procedures.

*Preparation of methyl 3'-((phenylsulfonyl)methyl)-[1,1'-biphenyl]-3-carboxylate (**5**)* A 500 mL Schlenk flask equipped with a reflux condenser and stir bar was charged with 1-bromo-3-((phenylsulfonyl)methyl)benzene (**3**) (4.81 g, 15.5 mmol), (3-(methoxycarbonyl)phenyl)boronic acid (**4**) (3.46 g, 19.2 mmol, 1.25 equiv.), $(PPh_3)_2PdCl_2$ (0.56 g, 0.8 mmol, 0.05 equiv.), and potassium carbonate (14.7 g, 107 mmol, 6.7 equiv.). Degassed 1:1 v/v H_2O:THF (200 mL) was added and the reaction mixture stirred for 16 h under N_2 at 90 °C. The reaction mixture was cooled to 24 °C and quenched with aqueous ammonium chloride (50 mL), extracted with EtOAc (2 × 25 mL), washed with water (50 mL) and brine (50 mL), dried with $MgSO_4$ and concentrated on a rotary evaporator. The dark brown solid was taken up in hot EtOAc (50 mL), filtered through celite to remove insoluble material, and evaporated. The residue was recrystallized from minimal EtOAc/hexane (1:1) and washed with hexane to give **3** (6.0 g, 15.5 mmol, 99%) as light brown needles. ^{1}H NMR (500 MHz, $CDCl_3$) δ = 8.05 (s, 1H), 8.01 (d, *J* = 7.8 Hz, 1H), 7.69 – 7.66 (m, 2H), 7.66 – 7.59 (m, 2H), 7.56 (d, *J* = 7.8 Hz, 1H), 7.48 (t, *J* = 7.7 Hz, 3H), 7.37 (t, *J* = 7.7 Hz, 1H), 7.21 (s, 1H), 7.16 (d, *J* = 7.6 Hz, 1H), 4.38 (s, 2H), 3.96 (s, 3H) ppm. ^{13}C{^{1}H} NMR (126 MHz, $CDCl_3$) δ 167.0, 140.61, 140.59, 137.8, 134.0, 131.6, 130.8, 130.3, 129.7, 129.3, 129.1, 129.0, 129.0, 128.9, 128.8, 128.2, 127.7, 63.0, 52.4 ppm. HRMS (ESI-TOF) m/z: $[C_{21}H_{18}O_4S+Na]^+$ calcd. 389.0818; found 389.0814.

*4,8-Bis(phenylsulfonyl)-1,2,5,6(1,3)-tetrabenzenacycloocta-phane-3,7-dione (**6**)* An oven-dried 1 L Schlenk flask was charged under N_2 with **5** (1.46 g, 4 mmol) in dry THF (450 mL). This mixture was added dropwise by cannula over 8 h to a second 1 L oven-dried Schlenk flask charged under N_2 with LiHMDS (1 M in THF, 17.6 mL, 17.6 mmol, 4.4 equiv.) in dry THF (50 mL). When the addition was complete, the reaction mixture was quenched with saturated aqueous NH_4Cl (50 mL) and water (50 mL), extracted with EtOAc (2 × 50 mL), washed with brine (50 mL), dried with $MgSO_4$ and concentrated on a rotary evaportator to a beige solid. The solid was triturated with MeOH (20 mL), then $CHCl_3$ (25 mL) and dried in vacuo to give **6** (860 mg, 1.28 mmol, 64%) as a colorless solid. ^{1}H NMR (600 MHz, pyridine-d_5) δ = 8.82 (s, 2H), 8.72 (s, 2H), 8.09 (d, *J* = 8.0 Hz, 2H), 7.88 (d, *J* = 7.3 Hz, 4H), 7.86 (d, *J* = 7.8 Hz, 2H), 7.81 (d, *J* = 7.7 Hz, 2H), 7.49 – 7.40 (m, 6H), 7.35 – 7.28 (m, 6H), 7.08 (s, 2H) ppm. ^{13}C{^{1}H} NMR (151 MHz, pyridine-d_5) δ = 190.1, 141.7, 140.4, 139.5, 137.0, 134.7, 132.1, 132.0, 131.9, 131.0, 130.8, 130.6, 130.5, 129.6, 129.4, 129.2, 128.2, 78.1 ppm. HRMS (ESI-TOF) m/z: $[C_{40}H_{28}O_6S_2+H]^+$ calcd. 667.1255; found 667.1265. The same reaction run at 400% scale (6.2 g **5**, 16 mmol) in the same volume of solvent gave **6** (2.15 g, 3.2 mmol) in 41% yield.

*1,2,5,6(1,3)-Tetrabenzenacyclooctaphane-3,7-dione (**7**)* A 25 mL soda-lime glass vial with a septum cap was charged with **6** (400 mg, 0.6 mmol), $Ru(bpy)_3Cl_2$ (13 mg, 0.02 mmol, 3.3 mol%), diethyl-2,6-dimethyl-1,4-dihydropyridine-3,5-dicarboxylate (334 mg, 1.32 mmol, 2.2 equiv.) in pyridine (20 mL). The reaction mixture was degassed by sparging with N_2 for 20 min and then irradiated by blue LED light (Westinghouse 0315100 15W PAR38 Outdoor LED flood light) for 16 h. When TLC (1:2:1 EtOAc:Hex:CH_2Cl_2, R_f: **6** = 0.40, **7** = 0.76) indicated reaction was complete, the dark red-orange reaction mixture was poured into H_2O (200 mL) and filtered through a pad of celite (2 cm × 5 cm dia). The filter cake was washed with H_2O until the filtrate was colorless (ca. 100 mL), then with MeOH until the filtrate was colorless (ca. 50 mL). The product was eluted from the filter cake with CH_2Cl_2 (300 mL), and concentrated on a rotary evaporator to give **7** (220 mg, 0.57 mmol, 94%) as a pale orange solid. ^{1}H NMR (600 MHz, $CDCl_3$) δ = 8.57 (s, 2H), 8.01 (s, 2H), 7.99 (d, *J* = 7.9 Hz, 2H), 7.78 (d, *J* = 7.5 Hz, 2H), 7.53 (t, *J* = 7.7 Hz, 2H), 7.43 – 7.32 (m, 7H), 4.39 (s, 4H) ppm. ^{13}C{^{1}H} NMR (151 MHz, $CDCl_3$) δ = 196.7, 141.0, 140.5, 137.5, 136.3, 130.68 , 129.9, 129.7, 129.2, 128.1, 127.5, 126.0, 49.3 ppm. HRMS (EI) m/z: $[C_{28}H_{20}O_2]^+$ calcd. 388.1463; found 338.1463.

*1,2,5,6(1,3)-Tetrabenzenacyclooctaphane-3,7-diyne (**1**)* A 500 mL oven-dried Schlenk flask under N_2 was charged with **7** (754mg, 1.94 mmol) and N-phenyltriflimide (2.1 g, 6 mmol, 3 equiv.) in dry THF (150 mL). The reaction mixture was cooled to –78 °C and solid KHMDS (2.4 g, 12 mmol, 6 equiv.) was added in one portion. The reaction was stirred at –78 °C for 2 h and then warmed to 24 °C and quenched with H_2O (40 mL). The organic layer was separated and concentrated on a rotary evaporator. The wet residue was triturated with MeOH (20 mL) to give a colorless solid, which was extracted with hot pyridine (30 mL) and filtered. Recrystallization from pyridine at 0 °C gave **1** (380 mg, 1.08 mmol, 56%) as a colorless crystalline solid. The material is analytically pure, but its subsequent polymerization is more reproducible after a second recrystallization from anhydrous THF under N_2. ^{1}H NMR (600 MHz, $CDCl_3$) δ = 8.52 (t, *J* = 1.7 Hz, 4H), 7.73 – 7.71 (dm, *J* = 7.7 Hz, 4H), 7.46 (t, *J* = 7.7 Hz, 4H), 7.31 – 7.29 (dm, *J* = 7.7 Hz, 4H) ppm. HRMS (EI) m/z: $[C_{28}H_{16}]^+$ calcd. 352.1252; found 352.1257. Spectroscopic data are consistent with a previous report.[34] Colorless blocks, uniformly 180° twins but suitable for X-ray diffraction, were grown by slow cooling of a saturated benzene solution from 80 to 22 °C. **1** crystallizes in the triclinic space group P-1, *a* = 5.5153(2) Å, *b* = 15.9898(7) Å, *c* = 20.1319(5) Å, α = 97.836(3)°, β = 86.477(3)°, γ = 89.047(4)°, *Z* = 2, GOF on F^2 = 1.076, *R* indices (all data) R1 = 0.0645, wR2 = 0.1496. Solid **1** should be stored under N_2 but can be handled in air; signs of decomposition (yellow color, reduced solubility) develop over the course of several weeks when stored at ambient conditions.

*p**TolCMo[ONO]O**t**Bu (**2**)* In an N_2-filled glovebox a 20 mL vial was charged with *p*TolCMo(O^tBu)$_3$•$(DME)_{0.5}$ (254 mg, 0.55 mmol) in dry toluene (4 mL) and 6,6'-(pyridine-2,6-diyl)bis(2,4-di-tert-butylphenol) (**H$_2$[ONO]**) (244 mg, 0.5 mmol) in dry toluene (2 mL) was added dropwise over 1 min. After stirring for 15 min at 24 °C the volatiles were removed in vacuo. The brown residue was suspended in pentane (3 mL) and filtered. The yellow solid was washed with pentane (2 × 1 mL) and dried at for 18 h at 100 °C and 0.1 torr to give **2** (256 mg, 0.34 mmol, 68%) as a yellow powder. ^{1}H NMR (500 MHz, C_6D_6) δ = 7.74 (d, *J* = 2.4 Hz, 2H), 7.29 (d, *J* = 2.4 Hz, 2H), 7.23 (d, *J* = 7.9 Hz, 2H), 6.97 (t, *J* = 7.9 Hz, 1H), 6.51 (d, *J* = 8.0 Hz, 2H), 6.37 (d, *J* = 8.1 Hz, 2H), 1.85 – 1.76 (m, 30H), 1.39 (s, 18H) ppm. ^{13}C{^{1}H} NMR (126 MHz, $CDCl_3$) δ = 305.4, 163.0, 157.4, 142.2, 141.1, 137.9, 137.5, 137.1, 129.5, 127.8, 126.4, 125.7, 124.6, 123.0, 83.3, 35.8, 34.5, 33.0, 31.9, 30.7, 21.4 ppm. Anal. for [*p*TolCMo[ONO](O^{t}Bu)] calcd. C 71.31, H 7.85, N 1.85; found C 71.21, H 7.57, N 2.04. Orange blocks of **2**•^{t}**BuOH** suitable for X-ray analysis were grown at 24 °C by slow evaporation of a pentane solution of the crude mixture of DME and ^{t}BuOH solvates prior to desolvation. **2**•^{t}**BuOH** crystallizes in the monoclinic space group $P2_1/c$, *a* = 15.9057(6) Å, *b* = 15.2617(5) Å, *c* = 19.1797(7) Å, β = 93.394(2)°, *Z* = 4, GOF on F^2 = 1.077, *R* indices (all data) R1 = 0.0450, wR2 = 0.0966.

General procedure for ring-opening alkyne metathesis polymerization: In an N_2-filled glovebox a resealable Schlenk tube was charged with solid **1**, **2**, and Ph_3CH (internal standard). Freshly dried toluene (0.3 mL per mg **1**) was added and the flask was sealed, removed from the glovebox, and connected to a Schlenk line. The flask was immersed in a preheated 80 °C oil bath and stirred vigorously until all of **1** had dissolved (typically 2–3 min) at which point a 0.1 mL aliquot was taken, diluted with 0.5 mL dry C_6D_6 and analyzed by NMR to verify the initial ratio of **1**:**2**:Ph_3CH (by integration of the internal proton of **1** at 8.15 ppm, the upfield ^{t}Bu groups at 1.38 ppm for **2** and 1.32 ppm for the initiated catalyst species, and the methine of Ph_3CH at 5.41 ppm). When >90% conversion of **1** was reached (NMR) the reaction temperature was lowered to 55 °C and ynamine **8** (100 equiv. to **2**) in minimal dry toluene was added. The reaction was stirred at 55 °C for 24 h and then the catalyst was hydrolyzed by the addition of 1 M Bu_4NOH solution

in MeOH (100 equiv. to **2**) and stirred for 90 min at 80 °C. The reaction mixture was poured into 5 volumes of EtOH, filtered, washed with EtOH and hexane and dried in vacuo to give *poly*-**1** in > 90% yield.

General procedure for post-polymerization Diels-Alder annulation: A 0.5 mL microwave vial with a stir bar was charged under N_2 with *poly*-**1** (12 mg) and cyclopentadienone **9** (99 mg, 0.14 mmol, 2 equiv. per alkyne) in 0.45 g of dry 4:1 w/w Ph_2O:sulfolane. The vial was capped and heated to 250 °C in a microwave reactor for 12 h. The vial was brought back into the glove box, uncapped to vent the internal CO pressure, and re-capped. To ensure complete conversion, heating was continued for 36 h at 250 °C in a microwave reactor. After cooling to 24 °C, the reaction mixture was diluted with toluene (1 mL), poured into EtOH (20 mL), and filtered. The solid was re-dissolved in hexane (1 mL) and precipitated with acetone (15 mL) to remove unreacted **9** and its decomposition products. The resulting gummy latex was centrifuged and the supernatant decanted. The pellet was re-dissolved in hexane (1 mL) and precipitated in EtOH (20 mL), filtered, washed with EtOH (20 mL), and dried in vacuo at 100 °C to constant weight to give polyphenylene *poly*-**10** (49 mg, 83%) as a colorless solid. ^{1}H NMR (500 MHz, $CDCl_3$) δ =7.23 – 6.06 (m, 26H), 2.33 (s, 4H), 1.39 (s, 4H), 1.25 (s, 32H), 1.11 (s, 4H), 0.87 (s, 6H) ppm. $^{13}C\{^1H\}$ NMR (126 MHz, $CDCl_3$, 50 mM $Cr(acac)_3$) δ = 140.1 (br), 138.2 (br), 131.4 (br), 126.7 (br), 35.5, 32.1, 31.4, 29.9, 29.5, 29.1, 22.9, 14.3 ppm. ^{13}C SSNMR (^{1}H-^{13}C CP, 126 MHz, 12 kHz MAS) δ = 141.2, 139.2, 131.9, 126.9, 36.1, 32.7, 30.4, 23.4, 14.7 ppm.

*ROAMP-**cGNR*** A 600 mL Schlenk flask was charged under N_2 with *poly*-**10** (62 mg) in dry CH_2Cl_2 (350 mL). The reaction mixture was vigorously sparged with N_2 for 15 min. $FeCl_3$ (1.27 g, 7.8 mmol, 7 equiv. per H) dissolved in 10 mL dry $MeNO_2$ was added and the reaction mixture was stirred at 24 °C for 84 h, continuously sparging with CH_2Cl_2-saturated N_2. When HCl evolution had ceased, the reaction was quenched by the addition of MeOH (200 mL) and filtered. The black solid was washed with MeOH (200 mL), 0.5 M HCl in 50% aqueous MeOH (100 mL), 1 M HCl (100 mL), deionized H_2O (200 mL), acetone (200 mL), EtOAc (200 mL), and hexane (100 mL). The solid was re-suspended by a 15-min sonication in toluene (100 mL), filtered, washed with toluene (100 mL) and CH_2Cl_2 (200 mL). The solid was re-suspended by a 15-minute sonication in EtOH (100 mL), filtered, washed with EtOH (100 mL) and MeOH (200 mL) and dried in vacuo at 100 °C to constant weight to give ROAMP-**cGNR** (61 mg, 99%) as a black solid. ^{13}C SSNMR (^{1}H-^{13}C CP, 126 MHz, 12 kHz MAS, 50%wt in KBr) δ = 138.6, 126.8, 122.5, 28.8, 13.2 ppm. Raman (powder, λ = 514 nm) 1325 (D), 1610 (G), 2637 (2D), 2933 (D+G) cm^{-1}.

ASSOCIATED CONTENT

Supporting Information

The Supporting Information is available free of charge on the ACS Publications website at DOI: 10.1021/jacs.XXXXXXX

Figures S1 to S3, methods and instrumentation, synthetic procedures for **8,** *p*TolCMo(O^{t}Bu)$_3$•(DME)$_{0.5}$ and **H$_2$[ONO]**, model studies for the regioselective cyclodehydrogenation of *poly*-**10**, X-ray crystallographic data (Figures S4 and S5, Tables S1 to S8), and NMR spectra (Figures S6 to S31).

X-ray data for **1** (CIF)

X-ray data for **2•^{t}BuOH** (CIF)

AUTHOR INFORMATION

Corresponding Author

* ffischer@berkeley.edu

ACKNOWLEDGMENT

Research supported by the National Science Foundation under contract number CHE-1455289 (ROAMP catalyst design and synthesis), the Office of Naval Research MURI Program under contract number N00014-16-1-2921 (GNR synthesis and characterization), S.v.K. and C.T.E. acknowledge support through the E^{3}S National Science Foundation REU program (ECCS-0939514). Berkeley NMR Facility is supported in part by NIH grants 1S10RR016634-01, SRR023679A, and S10OD024998, and X-Ray Facility is supported in part by NIH Shared Instrumentation Grant S10-RR027172. The authors acknowledge Dr. Hasan Celik for support with NMR acquisition, Dr. Nicholas Settineri for assistance with X-ray analysis, and the group of Prof. R. Sarpong for the extended use of their microwave reactor.

REFERENCES

(1) Wang, X.-Y.; Narita, A.; Müllen, K. Precision Synthesis versus Bulk-Scale Fabrication of Graphenes. *Nat. Rev. Chem.* **2018**, *2* (1), 0100.

(2) Müllen, K. Graphene as a Target for Polymer Synthesis. In *Hierarchical Macromolecular Structures: 60 Years after the Staudinger Nobel Prize II*; Percec, V., Ed.; Advances in Polymer Science; Springer International Publishing, 2013; pp 61–92.

(3) Yang, L.; Park, C.-H.; Son, Y.-W.; Cohen, M. L.; Louie, S. G. Quasiparticle Energies and Band Gaps in Graphene Nanoribbons. *Phys. Rev. Lett.* **2007**, *99* (18), 186801.

(4) Chen, Y.-C.; de Oteyza, D. G.; Pedramrazi, Z.; Chen, C.; Fischer, F. R.; Crommie, M. F. Tuning the Band Gap of Graphene Nanoribbons Synthesized from Molecular Precursors. *ACS Nano* **2013**, *7* (7), 6123–6128.

(5) Chen, Z.; Wang, H. I.; Bilbao, N.; Teyssandier, J.; Prechtl, T.; Cavani, N.; Tries, A.; Biagi, R.; De Renzi, V.; Feng, X.; Kläui, M.; De Feyter, S.; Bonn, M.; Narita, A.; Müllen, K. Lateral Fusion of Chemical Vapor Deposited N = 5 Armchair Graphene Nanoribbons. *J. Am. Chem. Soc.* **2017**, *139* (28), 9483–9486.

(6) Bronner, C.; Stremlau, S.; Gille, M.; Brauße, F.; Haase, A.; Hecht, S.; Tegeder, P. Aligning the Band Gap of Graphene Nanoribbons by Monomer Doping. *Angew. Chem. Int. Ed.* **2013**, *52* (16), 4422–4425.

(7) Vo, T. H.; Shekhirev, M.; Kunkel, D. A.; Orange, F.; Guinel, M. J.-F.; Enders, A.; Sinitskii, A. Bottom-up Solution Synthesis of Narrow Nitrogen-Doped Graphene Nanoribbons. *Chem. Commun.* **2014**, *50* (32), 4172–4174.

(8) Cloke, R. R.; Marangoni, T.; Nguyen, G. D.; Joshi, T.; Rizzo, D. J.; Bronner, C.; Cao, T.; Louie, S. G.; Crommie, M. F.; Fischer, F. R. Site-Specific Substitutional Boron Doping of Semiconducting Armchair Graphene Nanoribbons. *J. Am. Chem. Soc.* **2015**, *137* (28), 8872–8875.

(9) Durr, R. A.; Haberer, D.; Lee, Y.-L.; Blackwell, R.; Kalayjian, A. M.; Marangoni, T.; Ihm, J.; Louie, S. G.; Fischer, F. R. Orbitally Matched Edge-Doping in Graphene Nanoribbons. *J. Am. Chem. Soc.* **2018**, *140* (2), 807–813.

(10) Ruffieux, P.; Wang, S.; Yang, B.; Sánchez-Sánchez, C.; Liu, J.; Dienel, T.; Talirz, L.; Shinde, P.; Pignedoli, C. A.; Passerone, D.; Dumslaff, T.; Feng, X.; Müllen, K.; Fasel, R. On-Surface Synthesis of Graphene Nanoribbons with Zigzag Edge Topology. *Nature* **2016**, *531* (7595), 489–492.

(11) de Oteyza, D. G.; García-Lekue, A.; Vilas-Varela, M.; Merino-Díez, N.; Carbonell-Sanromà, E.; Corso, M.; Vasseur, G.; Rogero, C.; Guitián, E.; Pascual, J. I.; Ortega, J. E.; Wakayama, Y.; Peña, D. Substrate-Independent Growth of Atomically Precise Chiral Graphene Nanoribbons. *ACS Nano* **2016**, *10* (9), 9000–9008.

(12) Rizzo, D. J.; Veber, G.; Cao, T.; Bronner, C.; Chen, T.; Zhao, F.; Rodriguez, H.; Louie, S. G.; Crommie, M. F.; Fischer, F. R. Topological Band Engineering of Graphene Nanoribbons. *Nature* **2018**, *560* (7717), 204–208.

(13) Gröning, O.; Wang, S.; Yao, X.; Pignedoli, C. A.; Barin, G. B.; Daniels, C.; Cupo, A.; Meunier, V.; Feng, X.; Narita, A.; Müllen, K.; Ruffieux, P.; Fasel, R. Engineering of Robust Topological Quantum Phases in Graphene Nanoribbons. *Nature* **2018**, *560* (7717), 209–213.

(14) Goldhaber-Gordon, D.; Montemerlo, M. S.; Love, J. C.; Opiteck, G. J.; Ellenbogen, J. C. Overview of Nanoelectronic Devices. *Proc. IEEE* **1997**, *85* (4), 521–540.

(15) Zhao, P.; Chauhan, J.; Guo, J. Computational Study of Tunneling Transistor Based on Graphene Nanoribbon. *Nano Lett.* **2009**, *9* (2), 684–688.

(16) Nguyen, G. D.; Tsai, H.-Z.; Omrani, A. A.; Marangoni, T.; Wu, M.; Rizzo, D. J.; Rodgers, G. F.; Cloke, R. R.; Durr, R. A.; Sakai, Y.; Liou, F.;

Aikawa, A. S.; Chelikowsky, J. R.; Louie, S. G.; Fischer, F. R.; Crommie, M. F. Atomically Precise Graphene Nanoribbon Heterojunctions from a Single Molecular Precursor. *Nat. Nanotechnol.* **2017**, *12* (11), 1077–1082.

(17) Bronner, C.; Durr, R. A.; Rizzo, D. J.; Lee, Y.-L.; Marangoni, T.; Kalayjian, A. M.; Rodriguez, H.; Zhao, W.; Louie, S. G.; Fischer, F. R.; Crommie, M. F. Hierarchical On-Surface Synthesis of Graphene Nanoribbon Heterojunctions. *ACS Nano* **2018**, *12* (3), 2193–2200.

(18) Shekhirev, M.; Sinitskii, A. Solution Synthesis of Atomically Precise Graphene Nanoribbons. *Phys. Sci. Rev.* **2017**, *2* (5).

(19) Bielawski, C. W.; Grubbs, R. H. Living Ring-Opening Metathesis Polymerization. *Prog. Polym. Sci.* **2007**, *32* (1), 1–29.

(20) Chen, P. Designing Sequence Selectivity into a Ring-Opening Metathesis Polymerization Catalyst. *Acc. Chem. Res.* **2016**, *49* (5), 1052–1060.

(21) Bielawski, C. W.; Benitez, D.; Grubbs, R. H. An "Endless" Route to Cyclic Polymers. *Science* **2002**, *297* (5589), 2041–2044.

(22) von Kugelgen, S.; Bellone, D. E.; Cloke, R. R.; Perkins, W. S.; Fischer, F. R. Initiator Control of Conjugated Polymer Topology in Ring-Opening Alkyne Metathesis Polymerization. *J. Am. Chem. Soc.* **2016**, *138* (19), 6234–6239.

(23) Schrock, R. R. Synthesis of Stereoregular Polymers through Ring-Opening Metathesis Polymerization. *Acc. Chem. Res.* **2014**, *47* (8), 2457–2466.

(24) Xia, Y.; Olsen, B. D.; Kornfield, J. A.; Grubbs, R. H. Efficient Synthesis of Narrowly Dispersed Brush Copolymers and Study of Their Assemblies: The Importance of Side Chain Arrangement. *J. Am. Chem. Soc.* **2009**, *131* (51), 18525–18532.

(25) Wright, D. B.; Touve, M. A.; Adamiak, L.; Gianneschi, N. C. ROMPISA: Ring-Opening Metathesis Polymerization-Induced Self-Assembly. *ACS Macro Lett.* **2017**, *6* (9), 925–929.

(26) Boyd, T. J.; Schrock, R. R. Sulfonation and Epoxidation of Substituted Polynorbornenes and Construction of Light-Emitting Devices. *Macromolecules* **1999**, *32* (20), 6608–6618.

(27) Meier, S.; Reisinger, H.; Haag, R.; Mecking, S.; Mülhaupt, R.; Stelzer, F. Carbohydrate Analogue Polymers by Ring Opening Metathesis Poymerisation (ROMP) and Subsequent Catalytic Dihydroxylation. *Chem. Commun.* **2001**, No. 9, 855–856.

(28) Hensbergen, J. A. van; Burford, R. P.; Lowe, A. B. Post-Functionalization of a ROMP Polymer Backbone via Radical Thiol-Ene Coupling Chemistry. *J. Polym. Sci. Part Polym. Chem.* **2012**, *51* (3), 487–492.

(29) Jordan, R. S.; Wang, Y.; McCurdy, R. D.; Yeung, M. T.; Marsh, K. L.; Khan, S. I.; Kaner, R. B.; Rubin, Y. Synthesis of Graphene Nanoribbons via the Topochemical Polymerization and Subsequent Aromatization of a Diacetylene Precursor. *Chem* **2016**, *1* (1), 78–90.

(30) Jordan, R. S.; Li, Y. L.; Lin, C.-W.; McCurdy, R. D.; Lin, J. B.; Brosmer, J. L.; Marsh, K. L.; Khan, S. I.; Houk, K. N.; Kaner, R. B.; Rubin, Y. Synthesis of N = 8 Armchair Graphene Nanoribbons from Four Distinct Polydiacetylenes. *J. Am. Chem. Soc.* **2017**, *139* (44), 15878–15890.

(31) Hein, S. J.; Lehnherr, D.; Arslan, H.; J. Uribe-Romo, F.; Dichtel, W. R. Alkyne Benzannulation Reactions for the Synthesis of Novel Aromatic Architectures. *Acc. Chem. Res.* **2017**, *50* (11), 2776–2788.

(32) Hou, I. C.-Y.; Hu, Y.; Narita, A.; Müllen, K. Diels–Alder Polymerization: A Versatile Synthetic Method toward Functional Polyphenylenes, Ladder Polymers and Graphene Nanoribbons. *Polym. J.* **2018**, *50* (1), 3–20.

(33) Alabugin, I. V.; Gonzalez-Rodriguez, E. Alkyne Origami: Folding Oligoalkynes into Polyaromatics. *Acc. Chem. Res.* **2018**, *51* (5), 1206–1219.

(34) Utsumi, K.; Kawase, T.; Oda, M. [2.0.2.0]Metacyclophane-1,15-Diynes. A Potential Fragment of Double-Helical Conjugated Systems. *Chem. Lett.* **2003**, *32* (4), 412–413.

(35) Fischer, F. R.; Nuckolls, C. Design of Living Ring-Opening Alkyne Metathesis. *Angew. Chem. Int. Ed.* **2010**, *49* (40), 7257–7260.

(36) Sedbrook, D. F.; Paley, D. W.; Steigerwald, M. L.; Nuckolls, C.; Fischer, F. R. Bidentate Phenoxides as Ideal Activating Ligands for Living Ring-Opening Alkyne Metathesis Polymerization. *Macromolecules* **2012**, *45* (12), 5040–5044.

(37) Paley, D. W.; Sedbrook, D. F.; Decatur, J.; Fischer, F. R.; Steigerwald, M. L.; Nuckolls, C. Alcohol-Promoted Ring-Opening Alkyne Metathesis Polymerization. *Angew. Chem. Int. Ed.* **2013**, *52* (17), 4591–4594.

(38) Bellone, D. E.; Bours, J.; Menke, E. H.; Fischer, F. R. Highly Selective Molybdenum ONO Pincer Complex Initiates the Living Ring-Opening Metathesis Polymerization of Strained Alkynes with Exceptionally Low Polydispersity Indices. *J. Am. Chem. Soc.* **2015**, *137* (2), 850–856.

(39) von Kugelgen, S.; Sifri, R.; Bellone, D.; Fischer, F. R. Regioselective Carbyne Transfer to Ring-Opening Alkyne Metathesis Initiators Gives Access to Telechelic Polymers. *J. Am. Chem. Soc.* **2017**, *139* (22), 7577–7585.

(40) Jeong, H.; von Kugelgen, S.; Bellone, D.; Fischer, F. R. Regioselective Termination Reagents for Ring-Opening Alkyne Metathesis Polymerization. *J. Am. Chem. Soc.* **2017**, *139* (43), 15509–15514.

(41) Sedláček, J.; Sokol, J.; Zedník, J.; Faukner, T.; Kubů, M.; Brus, J.; Trhlíková, O. Homo- and Copolycyclotrimerization of Aromatic Internal Diynes Catalyzed with $Co_2(CO)_8$: A Facile Route to Microporous Photoluminescent Polyphenylenes with Hyperbranched or Crosslinked Architecture. *Macromol. Rapid Commun.* **2017**, *39* (4), 1700518.

(42) Vo, T. H.; Shekhirev, M.; Kunkel, D. A.; Morton, M. D.; Berglund, E.; Kong, L.; Wilson, P. M.; Dowben, P. A.; Enders, A.; Sinitskii, A. Large-Scale Solution Synthesis of Narrow Graphene Nanoribbons. *Nat. Commun.* **2014**, *5*, 3189.

(43) Cai, J.; Ruffieux, P.; Jaafar, R.; Bieri, M.; Braun, T.; Blankenburg, S.; Muoth, M.; Seitsonen, A. P.; Saleh, M.; Feng, X.; Müllen, K.; Fasel, R. Atomically Precise Bottom-up Fabrication of Graphene Nanoribbons. *Nature* **2010**, *466* (7305), 470–473.

(44) Orita, A.; An, D. L.; Nakano, T.; Yaruva, J.; Ma, N.; Otera, J. Sulfoximine Version of Double Elimination Protocol for Synthesis of Chiral Acetylenic Cyclophanes. *Chem. – Eur. J.* **2002**, *8* (9), 2005–2010.

(45) Jonathan, P. H.; Fukushima, T.; Kin, T.; Ogawa, A.; Aida, T. Amphipathic Hexa-Peri-Hexabenzocoronene Derivative. JP4005571, August 21, 2007.

(46) Gröber, S.; Görls, H.; Weigand, W. Photochemical Carbon–Carbon Bond Cleavage of CF_3-Substituted (Dppbe)Pt^0(H_2-Tolane) Complexes. *Eur. J. Inorg. Chem.* **2015**, *2015* (1), 149–155.

[TOC Graphic here]